Journal of Advanced Ceramics
2020, **9**(2): 232–242
https://doi.org/10.1007/s40145-020-0363-z
ISSN 2226-4108
CN 10-1154/TQ

Research Article

Microstructure modification of Y_2O_3 stabilized ZrO_2 thermal barrier coatings by laser glazing and the effects on the hot corrosion resistance

Lei GUO[a,b,*], Hui XIN[a], Zhao ZHANG[c], Xinmu ZHANG[a], Fuxing YE[a,b]

[a]*School of Materials Science and Engineering, Tianjin University, Tianjin 300072, China*
[b]*Tianjin Key Laboratory of Advanced Joining Technology, Key Lab of Advanced Ceramics and Machining Technology of Ministry of Education, Tianjin 300072, China*
[c]*School of Materials Science and Engineering, Liaocheng University, Liaocheng 252059, China*

Received: August 13, 2019; Revised: January 3, 2020; Accepted: January 14, 2020

Abstract: Y_2O_3 stabilized ZrO_2 (YSZ) thermal barrier coatings (TBCs) are prone to hot corrosion by molten salts. In this study, the microstructure of atmospheric plasma spraying YSZ TBCs is modified by laser glazing in order to improve the corrosion resistance. By optimizing the laser parameters, a ~18 μm smooth glazed layer with some vertical cracks was produced on the coating surfaces. The as-sprayed and modified coatings were both exposed to hot corrosion tests at 700 and 1000 ℃ for 4 h in V_2O_5 molten salt, and the results revealed that the modified one had improved corrosion resistance. After hot corrosion, the glazed layer kept structural integrity, with little evidence of dissolution. However, the vertical cracks in the glazed layer acted as the paths for molten salt penetration, accelerating the corrosion of the non-modified coating. Further optimization of the glazed layer is needed in the future work.

Keywords: thermal barrier coatings (TBCs); air plasma spraying (APS); Y_2O_3 stabilized ZrO_2; microstructure modification; laser glazing; V_2O_5 corrosion

1 Introduction

To improve the thermal efficiency and performance of turbine engines, thermal barrier coatings (TBCs) have been widely used on the hot section components of engines [1–3]. Typically, a TBC system consists of a ceramic top coat, commonly made of Y_2O_3 partially stabilized ZrO_2 (YSZ), a metallic bond coat that is resistant to oxidation, a thermally grown oxide (TGO) layer, and a substrate [4–6]. The ceramic top coat is for thermal insulation, usually produced by atmospheric plasma spraying (APS) with a splat microstructure and electron beam physical vapor deposition (EB-PVD) with a columnar microstructure [7–10].

TBCs are usually serviced in a corrosive environment, such as the use of poor-quality fuels containing V, Na, and S for turbine engines [11–13]. YSZ coatings are sensitive to molten salt corrosion. Corrosive mediums react with YSZ, leaching out the stabilizer Y_2O_3. As a result, the coating transforms from a metastable tetragonal (t') phase to a monoclinic phase, accompanied by a large volume expansion [13–16]. This causes cracks and

* Corresponding author.
E-mail: glei028@tju.edu.cn

destroys coating microstructures, resulting in a failure of TBCs. Therefore, much attempt has been made to develop solutions to suppress molten salt corrosion to TBCs and to improve the hot corrosion resistance.

Some strategies have been proposed to develop TBCs resistant to molten salt corrosion. One is to optimize coating compositions, for example, selecting more acidic oxides as the stabilizer for ZrO_2-based materials, such as Sc_2O_3, CeO_2, and TiO_2 [12,17,18], or developing new TBC materials to substitute for YSZ, and rare earth zirconates have been proposed as a series of promising materials [19,20]. Another approach is to tailor coating microstructures. Laser glazing has been considered as an effective method to densify the surfaces of APS coatings, reducing the specific surface area of coatings. As a result, the reaction between the coating and the molten salt is lowered, which leads to an enhanced corrosion resistance [21–24]. Additionally, a network of vertical cracks can be produced by laser glazing, which is beneficial to the thermal shock performance of coatings; on the other hand, it is also a path for molten salt penetration, harmful to the corrosion resistance [25–27]. Therefore, the microstructure optimization of the glazed layer on the coating surface is urgently needed.

The major aim of this work is to modify the surfaces of YSZ coatings by laser, optimizing the surface roughness, the vertical crack width, and the glazed layer thickness, and to investigate the effects of coating microstructure optimization on the hot corrosion behavior of YSZ coatings. Corrosion resistance to V_2O_5 molten salt of as-sprayed and laser modified YSZ coatings was compared, and the hot corrosion tests were conducted at 700 and 1000 ℃ for 4 h. Results indicated that the hot corrosion behavior of modified YSZ coatings at 700 and 1000 ℃ is different, and the related mechanisms are discussed. In the end, research on how to fully exploit advantages of the laser modification method to improve the hot corrosion resistance of TBCs is proposed.

2 Experimental procedure

2. 1 Materials

By the chemical co-precipitation and calcination method, 7wt% yttria partially stabilized zirconia (7YSZ) powders are obtained. The details about preparation process are available in our previous study [28]. To yield the desired result in the following spray process, the nano YSZ powders were agglomerated into microscopic particles by a spray drying method to improve the fluidity, and then sprayed onto graphite substrates by air plasma spraying (Metco 7M). The operating parameters are listed in Table 1, which are selected from the pre-optimization procedures.

2. 2 Laser glazing

A pulsed Nd:YAG laser system with a wavelength of 1064 nm (LWY-400, HGTECH, China) was employed for modifying surface microstructures of YSZ coatings, which is on operation by adjusting average power, scanning speed, pulse frequency, and spot diameter. The incidence angle of laser beam is 90°. The spot diameter is only adjusted by moving worktable up and down, which was ultimately determined as 1 mm by observing a single laser beam spot produced on the coating. In the process of laser glazing, in order to constrain the deformation of the coating and prevent the formation of large macroscopic cracks, the graphene substrate was reserved. In this study, the first laser glazed coating (LG-1) was fabricated by further optimization of parameters in our previous report [27], the whole surface area of which was treated by overlapping multiple parallel tracks with an overlap rate of 50%. Based on our observation and analysis of the thickness and the surface quality (smoothness and width of net-like cracks) of its re-melted layer, the process parameters are optimized again to produce the LG-2 coating. The process parameters of two sets of samples are listed in Table 2.

Table 1 Plasma spray parameters for the preparation of YSZ coatings

Current (A)	560
Voltage (V)	53
Primary gas, Ar (l/min)	40
Secondary gas, H_2 (l/min)	10
Feedstock giving rate (g/min)	22
Spray distance (mm)	100

Table 2 Process parameters to fabricate the laser glazed YSZ coatings

Parameter	LG-1	LG-2
Average power (W)	60	80
Pulse frequency (Hz)	15	20
Scanning speed (mm/s)	10	20
Spot diameter (mm)	1	1

2. 3 Hot corrosion tests

Hot corrosion tests of laser glazed coatings were conducted according to other researchers' experiments and our previous study [18,29]. Prior to the tests, the graphite substrate was removed to obtain free-standing ceramic coatings by holding isothermally 1 h at 800 ℃ in a box electric furnace (SX-1300 ℃), which has no effect on the results of following hot corrosion tests. Subsequently, V_2O_5 powders with a concentration of 10 mg/cm^2 were evenly spread on the coating surfaces by using a very flat potion spoon. The laser-glazed coatings covered with V_2O_5 were heat treated in a box electric furnace (SX-1300 ℃) at 700 and 1000 ℃ for 4 h. For comparison, as-sprayed coatings with V_2O_5 powders were also heat treated under the same conditions.

2. 4 Characterizations

X-ray diffractometer (XRD; Bruker D8 Advanced, Germany) using Cu Kα radiation was employed in determining phase constitution of the coatings, whose scanning range and rate were 10°–90° and 0.2 (°)/s, respectively. A digital microscope (VHX-2000C, KEYENCE, Japan) was adopted to measure the surface roughness of the laser glazed coating. The microstructure and chemical composition of the as-sprayed coatings, the laser-glazed coatings, and the V_2O_5-attacked coatings were examined by a scanning electron microscope (SEM; TDCLS4800, Hitachi Ltd., Japan) equipped with energy dispersive spectroscopy (EDS; IE 350).

3 Results and discussion

3. 1 Microstructure of the as-sprayed coating

Figure 1 shows the surface appearance, cross-section microstructure, and facture-section image of the as-sprayed YSZ coating. One could find melted splats (smooth zones), semi-melted particles, cracks, and pores on the coating surface, which are typical characteristics of APS coatings. During the plasma spraying process, coatings are exposed to large tensile stresses due to a rapid cooling rate, which causes some micro-cracks [30]. Cracks can improve the stress tolerance, which benefits the thermal shock performance of coatings. Additionally, cracks and pores have positive effects on the thermal insulation of coatings. Note that in the cross-section image, there are some grey contrasted zones, which correspond to semi-melted particles with sizes at the nanoscale. In Fig. 1(c), it could be found that mutual overlapped splats are evident, among which some porous zones evolving from non-molten particles exist. The porous zone is also denoted as the nanozone, which is composed of many fine particles. Some researchers indicate that a coating containing nanozones can be denoted as the nanostructured coating, and this type of coatings is reported to have a better corrosion resistance than their conventional counterparts [31,32].

3. 2 Coating microstructure modification by laser glazing

The coating surfaces are modified by laser glazing with two sets of different parameters, and surface and

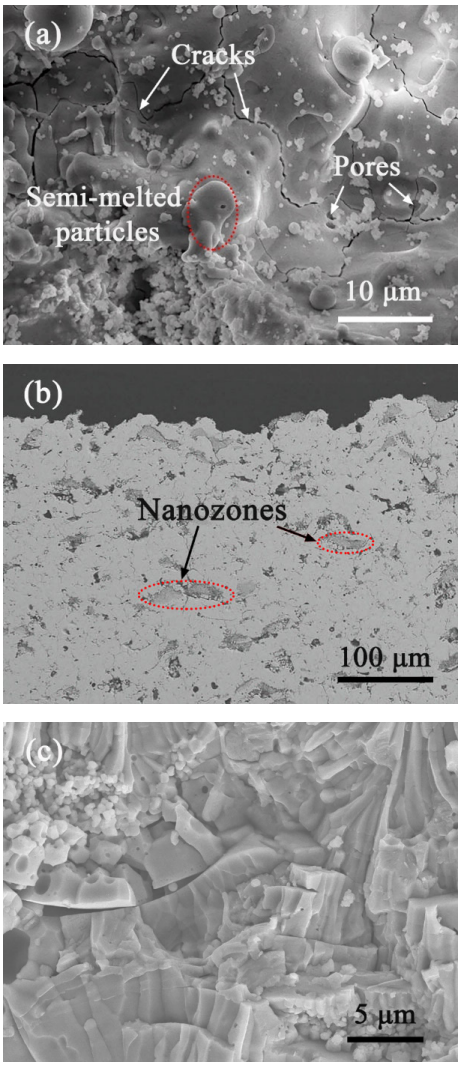

Fig. 1 (a) Surface appearance, (b) cross-section microstructure, and (c) facture-section image of the as-sprayed YSZ coating.

fracture-section images are presented in Fig. 2. Compared with the as-fabricated coating, the re-melted surfaces reveal significantly smoother morphologies, and most semi-melted particles on the surfaces have disappeared. Additionally, obvious net-like cracks are found on the coating surfaces. In the fracture sections (Figs. 2(b) and 2(d)), the laser glazed layers are found to have a dense columnar microstructure, with some vertical cracks penetrating through the thickness. The formation mechanism for net-like/vertical cracks can be understand as follows: since the energy of a laser spot is unevenly distributed (the center has a higher energy density), the energy input and the solidification speed of the laser spot covered region are inhomogeneous during the laser treatment; as a result, a large stress could be created in the re-melted region, causing net-like/vertical cracks [33,34]. Note that there are a few horizontal cracks at the interface between the glazed layer and the non-modified coating, which form to release the additional stress evolving from the large shrinkage of the re-melted layer and are undesirable for the coating applications.

In Figs. 2(a) and 2(b) (the LG-1 sample), one could find that the surface still has some obvious un-melted particles, and the crack width is large and the glazed layer is a little thick. It has been reported that smoother surfaces (lower specific surface area) of coatings are beneficial for corrosion resistance due to the reduced corrosion reaction between molten salts and the coating [22,26,35]. Large cracks are undesirable, which can act as the paths for molten salt penetration, and thick glazed layer is also detrimental which introduces large internal stress causing interface mismatch. To remove the un-melted particles to generate a smoother surface, the power and the pulse frequency were increased to produce higher energy to melt the upper coating. However, higher power and pulse frequency also mean a higher heat input, resulting in the formation of a thicker glazed layer. Therefore, in order to obtain moderate heat input, the corresponding scanning speed was also increased, which is conductive to reduce the glazed layer thickness. Comparing with the LG-1 sample, the LG-2 sample has a smoother surface, and its thickness and crack width are reduced, as shown in Figs. 2(c) and 2(d).

To better confirm that the sample with a smoother surface was obtained by optimizing parameters, a digital microscope was adopted to measure the surface roughness of the laser glazed coating (LG-1 and LG-2). Three-dimensional morphologies of the laser-glazed coating (LG-1 and LG-2) are presented in Fig. 3. The R_a value decreases from 2.86 μm for the LG-1 sample to 2.17 μm for the LG-2 sample. In addition, the width of net-like cracks on the LG-1 and LG-2 sample

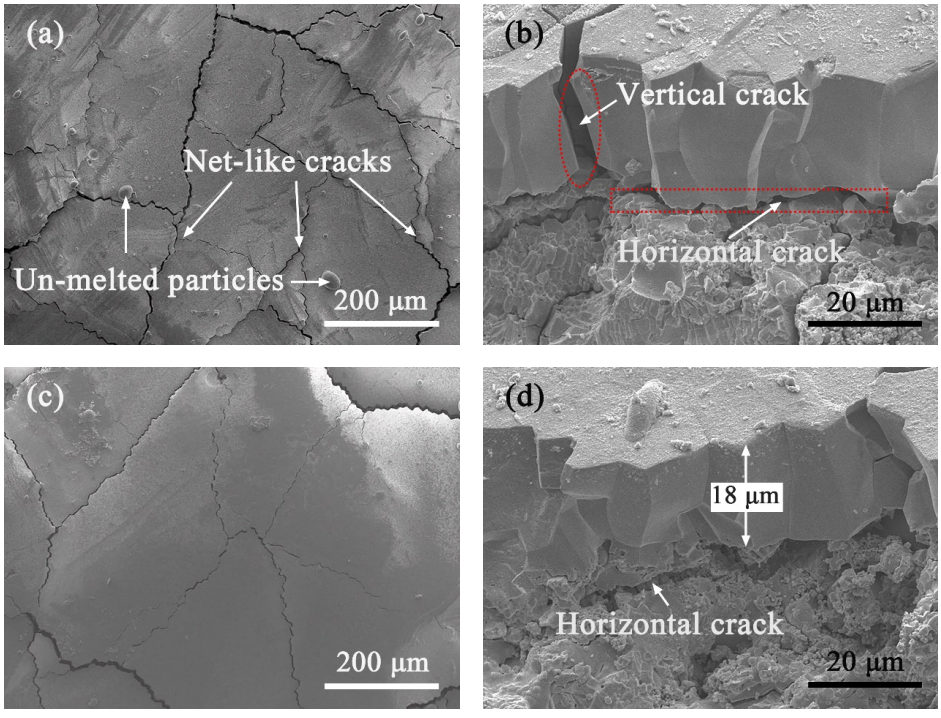

Fig. 2 (a, c) Surface and (b, d) fracture-section images of the laser glazed YSZ coatings: (a, b) LG-1, (c, d) LG-2.

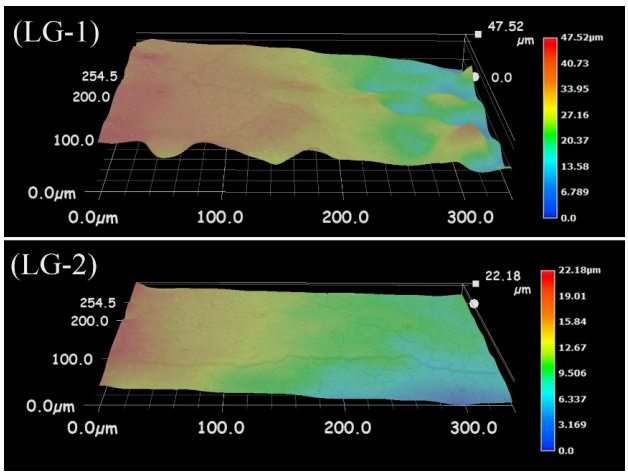

Fig. 3 Three-dimensional morphologies of the laser-glazed coatings (LG-1 and LG-2).

surface was also measured using a scanning electron microscope. 50 values for each of the LG-1 and LG-2 samples were collected by measuring the width of cracks in different regions of the coating, and then were averaged as 2.07 and 1.76 μm, respectively. Therefore, the LG-2 coatings are used for subsequent hot corrosion experiments.

The phase structure of the laser modified coating was measured by XRD, and the pattern is presented in Fig. 4, which also includes the XRD pattern of the as-sprayed coating. All the coatings are composed of t' phase. This type of phase is desirable for TBC applications due to its high toughness, good high-temperature stability, and low thermal conductivity, which can be obtained by rapid cooling [36,37]. Both APS and laser glazing have high cooling rates, up to 10^4 and 10^7 ℃/s, respectively [22]. Note that compared with the as-sprayed coating, the laser modified coating has intensified diffraction peaks at 2θ positions of 34.7° and 59.4°.

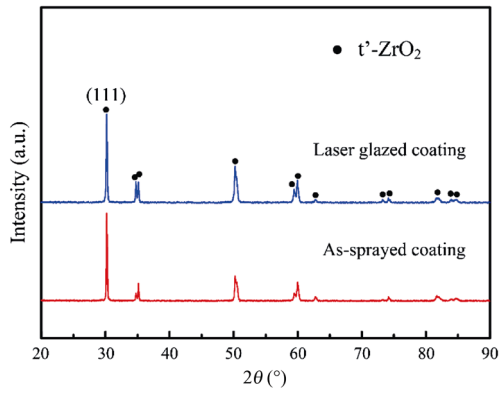

Fig. 4 XRD patterns of the as-sprayed and laser glazed YSZ coatings.

Research indicates that this phenomenon is attributed to the fact that the laser modified layer has reduced amounts of amorphous phases and reveals a preferential orientation of columnar microstructure [27].

3. 3 Hot corrosion behavior of YSZ coatings in V_2O_5 molten salt

3.3.1 Hot corrosion behavior of as-sprayed YSZ coatings

Figure 5 shows surface morphologies of as-sprayed YSZ coatings after hot corrosion tests at 700 and 1000 ℃. Large amounts of corrosion products are observed on the surfaces, which could be classified into two sets according to crystal shapes. In enlarged images as shown in Figs. 5(b) and 5(d), different shapes of corrosion products are marked as A, B, C, and D, and their chemical compositions were analyzed by EDS. Compound A contains V, Zr, and O, compounds B and D have Y, V, and O, and compound C is composed of 38.4 at% Zr, 60.9 at% O, and 0.7 at% Y, as listed in Table 3. To determine the phase compositions of these corrosion products, XRD analysis was carried out. Compared with the as-fabricated coating, the XRD patterns of the corroded coatings have many extra diffraction peaks, as shown in Fig. 6.

For the sample after the hot corrosion test at 700 ℃, XRD detects ZrV_2O_7, YVO_4, m-ZrO_2, and obvious t'-ZrO_2. For the coating corroded at a higher temperature (1000 ℃), only diffraction peaks ascribed to YVO_4 and m-ZrO_2 phases could be detected by XRD. The absence of t'-ZrO_2 in this corrosion condition indicates that the coating has been largely corroded by molten salts. In combination with the XRD and SEM results, one could confirm that crystals A and B in Fig. 5(b) are ZrV_2O_7 and YVO_4, respectively, while compounds C and D in Fig. 5(d) are m-ZrO_2 and YVO_4, respectively. Note that for the samples corroded at 700 ℃, XRD detects the presence of m-ZrO_2, but SEM does not, which might be attributed to its low content or being covered with ZrV_2O_7 and YVO_4 crystals.

Figure 7 shows the cross-sectional images of YSZ coatings after hot corrosion at 700 and 1000 ℃ and the corresponding V distribution of figures. After hot corrosion at 700 ℃, a reaction layer with a grey contrast formed on the coating surface, mainly composed of ZrV_2O_7 by the above XRD and SEM analysis, which is also consistent with the mapping result presented in Fig. 7(b). Beneath the layer, the coating almost keeps

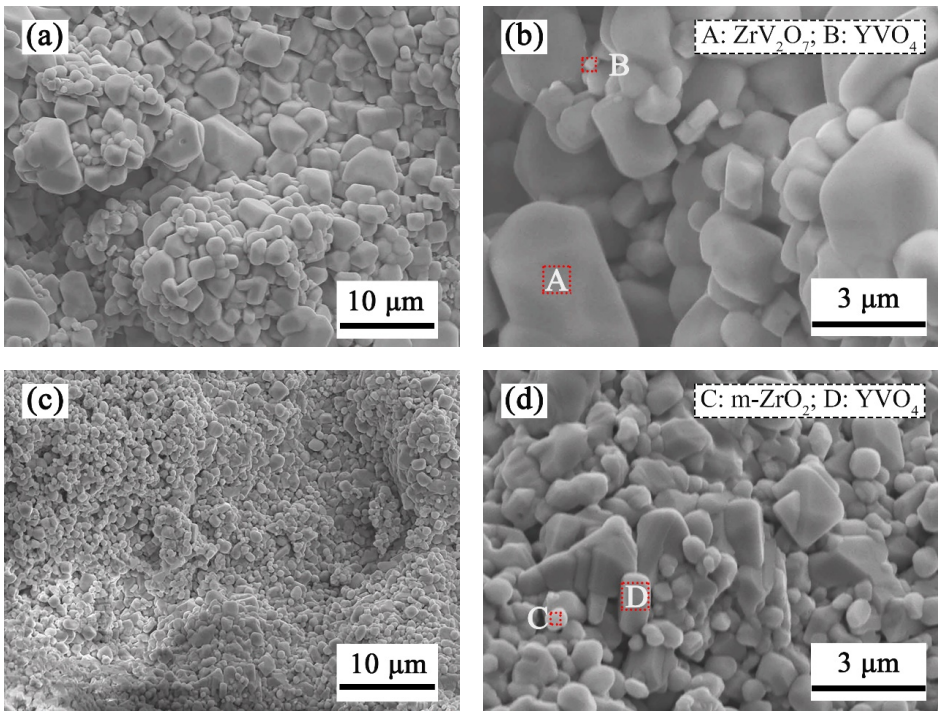

Fig. 5 Surface morphologies of the as-sprayed YSZ coatings after hot corrosion tests at (a, b) 700 ℃ and (c, d) 1000 ℃.

Table 3 Chemical compositions of the different regions A–D in Fig. 5

	Zr (at%)	V (at%)	O (at%)	Y (at%)
A	15.2	25.5	59.3	—
B	—	15.7	71.8	12.5
C	38.4	—	60.9	0.7
D	—	18.0	66.8	15.2

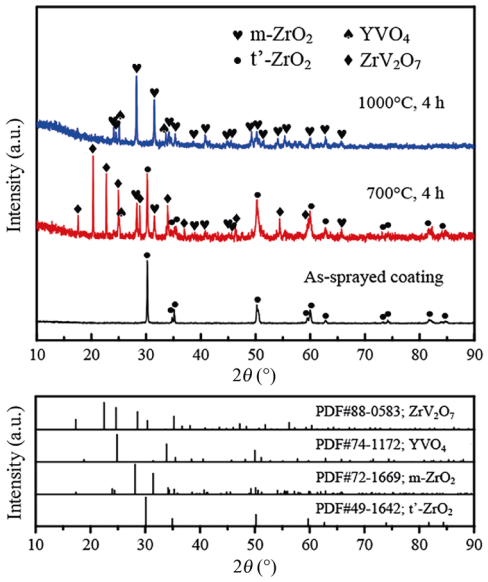

Fig. 6 XRD patterns of the as-sprayed YSZ coatings after hot corrosion tests. The standard PDF cards of ZrV_2O_7, YVO_4, m-ZrO_2, and t'-ZrO_2 are also presented.

its original microstructure; however, some obvious salt trace can be found in porous regions implying the penetration of molten salts, as shown in Fig. 7(b). After hot corrosion at 1000 ℃, it could be found that the coating microstructure has largely been destroyed by molten salt (Fig. 7(c)). By the observation on the V distribution presented in Fig. 7(d), the V_2O_5 molten salt diffusely distributed throughout the coating, suggesting the penetration became more serious. It is known that APS coatings have many pores and cracks, which provide the paths for molten salt penetration [34,38]. The melt point of V_2O_5 is 690 ℃, slightly lower than the corrosion temperature of 700 ℃, while at 1000 ℃, the temperature is high enough to melt the salt, leading to a rather low viscosity. Therefore, it is reasonable that the penetration of V_2O_5 molten salt became more serious in the coating corroded at 1000 ℃.

3.3.2 Hot corrosion behavior of laser glazed YSZ coatings

Figure 8 shows surface morphologies of the coatings after hot corrosion tests at 700 and 1000 ℃. Similar to the case of the as-sprayed coatings, the modified coatings are also covered by corrosion products. In Figs. 8(b) and 8(d) showing enlarged images of the coating surfaces, one could find that the corrosion products reveal several significantly different shapes, marked as A, B, C, and

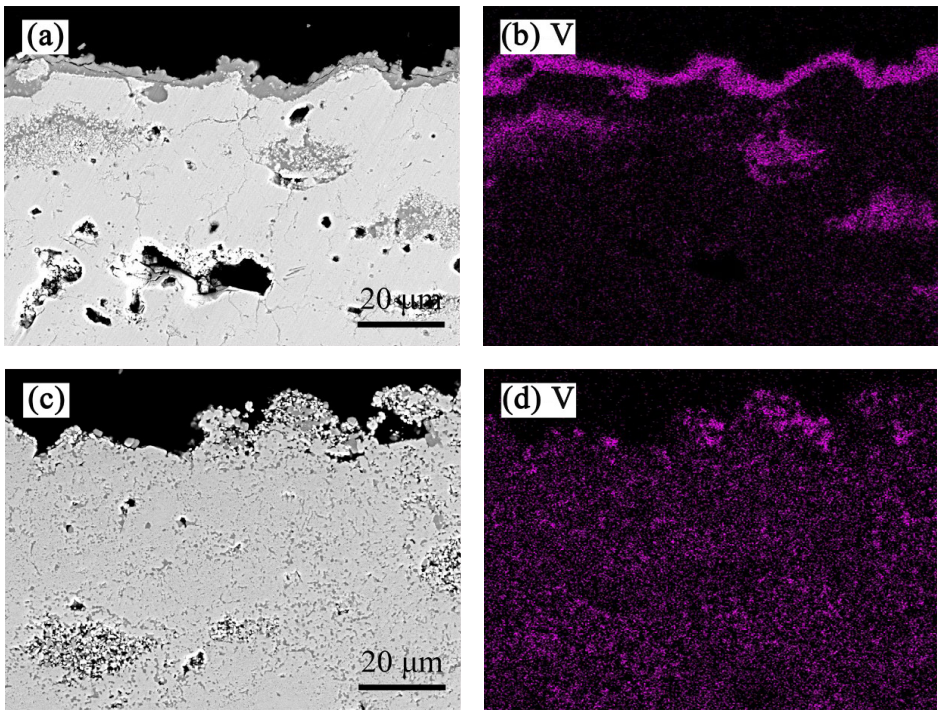

Fig. 7 Cross-sectional images of the as-sprayed YSZ coatings after hot corrosion at (a) 700 ℃ and (c) 1000 ℃. Figures (b) and (d) display the corresponding V distribution of figures (a) and (c), respectively.

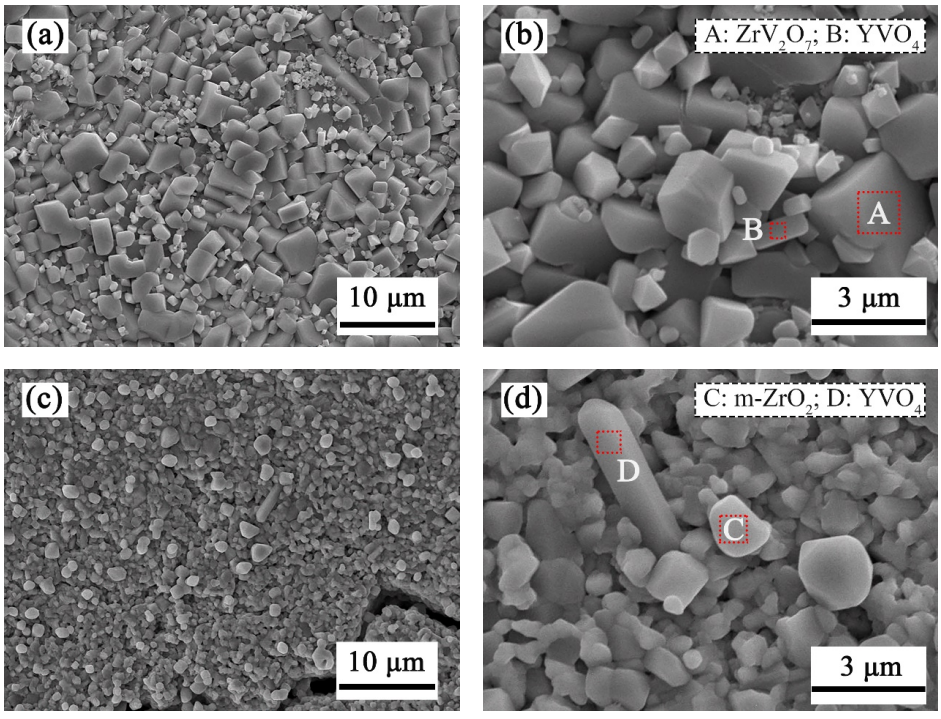

Fig. 8 Surface morphologies of the laser glazed YSZ coatings after hot corrosion tests at (a, b) 700 ℃ and (c, d) 1000 ℃.

D. The chemical compositions of these crystals are determined by EDS: crystal A has 12.2 at% Zr, 23.5 at% V, and 64.3 at% O, crystals B and D contain Y, V, and O, and crystal C consists of 32.6 at% Zr, 67.0 at% O, and 0.4 at% Y, as listed in Table 4.

XRD was used to confirm the phase structures of the corrosion products. In Fig. 9, ZrV_2O_7, YVO_4, t'-ZrO_2, and a little V_2O_5 are detected on the surface of

Table 4 Chemical compositions of the different regions A–D in Fig. 8

	Zr (at%)	V (at%)	O (at%)	Y (at%)
A	12.2	23.5	64.3	—
B	—	20.6	59.8	19.6
C	32.6	—	67.0	0.4
D	—	18.2	65.4	16.4

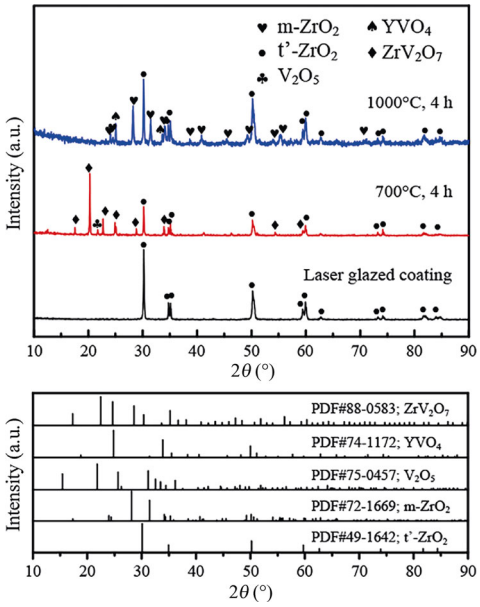

Fig. 9 XRD patterns of the laser glazed YSZ coatings after hot corrosion tests. The standard PDF cards of ZrV_2O_7, YVO_4, V_2O_5, m-ZrO_2, and t'-ZrO_2 are also presented.

the modified coating after corrosion at 700 ℃, while for the 1000 ℃ corrosion case, YVO_4, m-ZrO_2, and evident t'-ZrO_2 are identified. The detection of V_2O_5 in the former case indicates that V_2O_5 is hard to penetrate into and react with the modified coating; no V_2O_5 present on the coating surface after corrosion at 1000 ℃ might be due to the largely increased fluidity, which promotes the molten salt penetration. By comparison, SEM does not detect V_2O_5, which could be because that only a small amount of V_2O_5 remained or it permeated into deeper regions of the coating. Large amounts of t'-ZrO_2 remained after hot corrosion implies that the modified coating has a significantly improved phase stability in molten salt, which is desirable since an excellent phase stability is critical for TBC applications [23,39]. According to the XRD and EDS results, it can be identified the corrosion products in Fig. 8: crystals A and B in Fig. 8(b) are ZrV_2O_7 and YVO_4, respectively, whereas crystals C and D in Fig. 8(d) are m-ZrO_2 and YVO_4, respectively.

Figure 10 shows the cross-sectional microstructures of laser modified coatings after hot corrosion tests. It seems that the glazed layers still keep their dense columnar microstructures. For the case of corrosion at 700 ℃, a few amounts of corrosion products can be observed on the surface, and the vertical cracks become wider and longer, as shown in Fig. 10(a). This might be

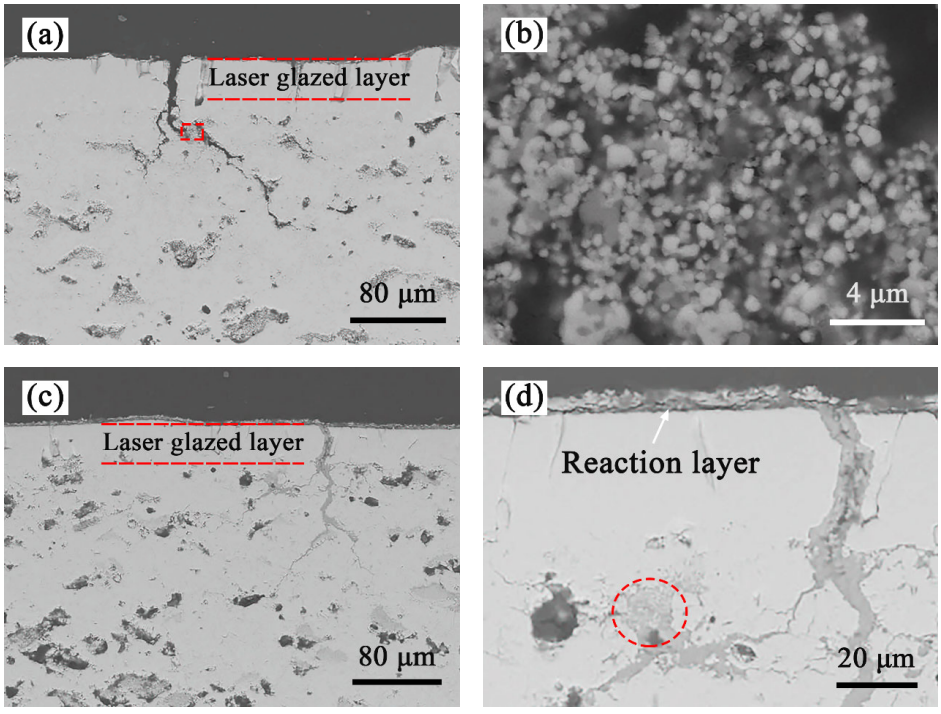

Fig. 10 Cross-sectional images of the laser glazed YSZ coatings after hot corrosion at (a, b) 700 ℃ and (c, d) 1000 ℃.

due to the dissolution of molten salt into the glazed layer, which can react with the coating. Since the corrosion temperature of 700 ℃ is just above the melting point of V_2O_5 (690 ℃), V_2O_5 molten salt has a low fluidity, and it cannot flow along the surface and vertical cracks freely. As a result, the salt can only react preferentially with the coating nearby compared with penetrating into the deeper region of the coating. The region highlighted by a red rectangle in Fig. 10(a) was observed at a higher degree of magnification, as shown in the inset image. It could be found that this region completely loses its original coating microstructure, indicative of severe reaction between the coating and the salt. This provides an evidence that at 700 ℃, molten salt mainly reacts with the region nearby, and even if it penetrates along vertical cracks, it prefers reaction rather than continuous penetration. The reaction causes phase transformation from t' to m phase, accompanied by about 5% volume expansion, which accelerates the degradation and spallation of the vertical cracks region near molten salt in coating and makes vertical cracks wider and longer.

Compared with the case of 700 ℃ corrosion, cross-sectional microstructure of the modified coating after corrosion at 1000 ℃ has some similarities and difference: both laser glazed layers keep structural integrity and have good adhesion to the non-modified coatings; the difference is that in Figs. 10(c) and 10(d) large amounts of corrosion products are observed on the surface, and the vertical cracks are filled with molten salt. The reasons for the difference could be provided as follows: at the corrosion temperature of 1000 ℃, the molten salt has a sufficiently low viscosity, which makes melt flow freely. In this case, molten salt is easy to be gathered in the vertical cracks. Since the laser glazed layer is rather immune to dissolution by molten salt, the salt stays in the cracks after cooling, as shown in Fig. 10(d). However, the regions around the cracks in the non-modified coating are severely destroyed by molten salt, as highlighted by a red circle in Fig. 10(d). Note that in Fig. 10(d), the corrosion products form a reaction layer with a thickness of ~5 μm, beneath which the glazed layer has little damage. Since the reaction layer is thin, X-ray can penetrate through it, and evident t'-ZrO_2 is detected, as shown in Fig. 9. An obvious delamination crack exists between the reaction layer and the coating, which is attributed to the thermal mismatch between these two layers.

3. 4 Corrosion mechanisms of as-sprayed and laser glazed coatings in V_2O_5 salts

The hot corrosion mechanisms of YSZ coatings have been investigated by some researchers, and our present work confirms the mechanisms: at temperatures above the melting point of V_2O_5, molten salts penetrate into the coating pores and cracks, and react with the YSZ coating, leaching out the stabilizer, which causes phase transformation and destroys the coating microstructures. In this study, the microstructures of as-sprayed coating have largely been destroyed by molten salt, which suggests that APS YSZ coatings are prone to hot corrosion by molten salts.

After hot corrosion tests at 700 and 1000 ℃, the corrosion products on the surfaces of laser modified coatings are similar to those of as-sprayed coatings, and the formation mechanisms are the same. The V_2O_5 melts at a temperature of 690 ℃, reacts with Y_2O_3 and ZrO_2 to form YVO_4 and ZrV_2O_7, respectively. This leads to the formation of m-ZrO_2 owing to the depletion of Y_2O_3 in ZrO_2. Therefore, at 700 ℃, the reaction equation could be given as follow:

$$V_2O_5(l) + ZrO_2(Y_2O_3)(s) \rightarrow YVO_4(s) + ZrV_2O_7(s) + m\text{-}ZrO_2(s) \quad (1)$$

ZrV_2O_7 is an intermediate compound in V_2O_5–ZrO_2 system, which melts incongruently at 747 ℃ to ZrO_2 and a V_2O_5-rich liquid [29]. The latter continues to react with Y_2O_3, reducing the content of V_2O_5 in V_2O_5-rich liquid, which accelerates the precipitation of m-ZrO_2. On the basis of the aforementioned analysis, the reaction mechanism between YSZ and V_2O_5 at 1000 ℃ could be represented by the following expression:

$$V_2O_5(l) + ZrO_2(Y_2O_3)(s) \rightarrow YVO_4(s) + m\text{-}ZrO_2(s) \quad (2)$$

However, by analyzing the coating microstructures after hot corrosion, one could find that APS YSZ coatings modified by laser glazing reveal significantly improved corrosion resistance to molten salts. The glazed layer has a smooth surface and dense microstructure, which cause molten salts hard to dissolve the coating. As a result, the glazed layer can survive the molten salt attack, keeping structural integrity. However, due to the vertical cracks generated during the laser glazing process, the molten salt has a large tendency to penetrate along these cracks, destroying the microstructure of the non-modified coating. The corrosion temperature also affects the hot corrosion behavior of the modified

coatings, which is a result of temperature related viscosity of molten salts.

Based on the above analysis, laser glazing is a promising technique for improving the hot corrosion resistance of TBCs. However, it also has some limitation. The glazed laser usually contains many vertical cracks, which provide the paths for molten salt penetration; if all the vertical cracks are removed, the glazed layer is easy to be spalled due to the dense microstructure. Therefore, to take advantages of this technique, the glazing parameters need further optimization and the coating microstructures should be designed; for example, the laser glazed layer is designed to be multiple sub-layers, making the vertical cracks in each sub-layer separated and thus no straight path existed for molten salt penetration. Our future work will be focused on this.

4 Conclusions

In this study, a laser glazing technique is employed to modify the microstructure of APS YSZ TBCs in order to improve the corrosion resistance of coatings. The as-sprayed and modified coatings were subjected to hot corrosion tests in the presence of V_2O_5 molten salt at 700 and 1000 ℃ for 4 h, and the corrosion products, microstructure evolution, and related mechanisms were investigated. The following conclusions could be drawn:

(1) Laser glazing can smooth the coating surface and cause a columnar microstructure with some vertical cracks. The crack width was optimized, and the glazed layer remained a t' phase with a thickness of ~18 μm.

(2) The modified coatings revealed a better resistance to molten salt corrosion than the as-sprayed coatings. Both two types of the coatings had similar corrosion products on the surfaces, mainly consisting of ZrV_2O_7 and YVO_4, and m-ZrO_2 and YVO_4 after corrosion at 700 and 1000 ℃, respectively. However, for the modified coatings after corrosion, large amounts of the t' phase were detected, indicative of excellent phase stability of the glazed layer.

(3) After corrosion, the microstructures of the as-sprayed coating were severely destroyed by molten salts, while those of the glazed layer on the modified coatings kept integrity.

(4) The vertical cracks in the glazed layers of modified coatings provided the paths for molten salt penetration. As a result, the regions around the vertical cracks and the non-modified coating were corroded by molten salts, which is harmful to the corrosion lifetime of the entire coating.

Laser glazing is a promising technique for improving corrosion resistance of TBCs in the presence of molten salt; however, for fully exploiting the advantages of this technique, glazing parameters and coating microstructures need further optimization.

Acknowledgements

This research is sponsored by the National Natural Science Foundation of China (Grant No. 51971156).

References

[1] Vaßen R, Jarligo MO, Steinke T, *et al*. Overview on advanced thermal barrier coatings. *Surf Coat Technol* 2010, **205**: 938–942.

[2] Liang PP, Dong SJ, Zeng JY, *et al*. $La_2Hf_2O_7$ ceramics as potential top-coat materials for thermal/environmental barrier coatings. *Ceram Int* 2019, **45**: 22432–22436.

[3] Cheng B, Yang GJ, Zhang Q, *et al*. Gradient thermal cyclic behaviour of $La_2Zr_2O_7$/YSZ DCL-TBCs with equivalent thermal insulation performance. *J Eur Ceram Soc* 2018, **38**: 1888–1896.

[4] Clarke DR, Oechsner M, Padture NP. Thermal-barrier coatings for more efficient gas-turbine engines. *MRS Bull* 2012, **37**: 891–898.

[5] Clarke DR, Phillpot SR. Thermal barrier coating materials. *Mater Today* 2005, **8**: 22–29.

[6] Mao WG, Wang YJ, Shi J, *et al*. Bending fracture behavior of freestanding $(Gd_{0.9}Yb_{0.1})_2Zr_2O_7$ coatings by using digital image correlation and FEM simulation with 3D geometrical reconstruction. *J Adv Ceram* 2019, **8**: 564–575.

[7] Li GR, Yang GJ. Understanding of degradation-resistant behavior of nanostructured thermal barrier coatings with bimodal structure. *J Mater Sci Technol* 2019, **35**: 231–238.

[8] Rätzer-Scheibe HJ, Schulz U. The effects of heat treatment and gas atmosphere on the thermal conductivity of APS and EB-PVD PYSZ thermal barrier coatings. *Surf Coat Technol* 2007, **201**: 7880–7888.

[9] Sampath S, Schulz U, Jarligo MO, *et al*. Processing science of advanced thermal-barrier systems. *MRS Bull* 2012, **37**: 903–910.

[10] Guo HB, Gong SK, Zhou CG, *et al*. Investigation on hot-fatigue behaviors of gradient thermal barrier coatings by EB-PVD. *Surf Coat Technol* 2001, **148**: 110–116.

[11] Chen XL, Zhao Y, Gu LJ, *et al*. Hot corrosion behaviour of plasma sprayed YSZ/$LaMgAl_{11}O_{19}$ composite coatings in molten sulfate–vanadate salt. *Corros Sci* 2011, **53**: 2335–2343.

[12] Liu HF, Xiong X, Li XB, *et al*. Hot corrosion behavior of Sc_2O_3–Y_2O_3–ZrO_2 thermal barrier coatings in presence of Na_2SO_4+V_2O_5 molten salt. *Corros Sci* 2014, **85**: 87–93.

[13] Guo L, Yan Z, Yu JX, *et al*. Hot corrosion behavior of TiO_2 doped, Yb_2O_3 stabilized zirconia exposed to V_2O_5 + Na_2SO_4

molten salt at 700–1000 ℃. *Ceram Int* 2018, **44**: 261–268.
[14] Afrasiabi A, Saremi M, Kobayashi A. A comparative study on hot corrosion resistance of three types of thermal barrier coatings: YSZ, YSZ+Al_2O_3 and YSZ/Al_2O_3. *Mat Sci Eng A* 2008, **478**: 264–269.
[15] Jamali H, Mozafarinia R, Shoja-Razavi R, *et al*. Comparison of hot corrosion behaviors of plasma-sprayed nanostructured and conventional YSZ thermal barrier coatings exposure to molten vanadium pentoxide and sodium sulfate. *J Eur Ceram Soc* 2014, **34**: 485–492.
[16] Sivakumar G, Banerjee S, Raja VS, *et al*. Hot corrosion behavior of plasma sprayed powder-solution precursor hybrid thermal barrier coatings. *Surf Coat Technol* 2018, **349**: 452–461.
[17] Habibi MH, Guo SM. The hot corrosion behavior of plasma sprayed zirconia coatings stabilized with yttria, ceria, and titania in sodium sulfate and vanadium oxide. *Mater Corros* 2015, **66**: 270–277.
[18] Loghman-Estarki MR, Shoja Razavi R, Edris H, *et al*. Comparison of hot corrosion behavior of nanostructured ScYSZ and YSZ thermal barrier coatings. *Ceram Int* 2016, **42**: 7432–7439.
[19] Li F, Zhou L, Liu JX, *et al*. High-entropy pyrochlores with low thermal conductivity for thermal barrier coating materials. *J Adv Ceram* 2019, **8**: 576–582.
[20] Zhu RB, Zou JP, Mao J, *et al.* Fabrication and growing kinetics of highly dispersed gadolinium zirconate nanoparticles. *Research and Application of Materials Science* 2019, **1**: 28–34.
[21] Tsai PC, Lee JH, Hsu CS. Hot corrosion behavior of laser-glazed plasma-sprayed yttria-stabilized zirconia thermal barrier coatings in the presence of V_2O_5. *Surf Coat Technol* 2007, **201**: 5143–5147.
[22] Ghasemi R, Shoja-Razavi R, Mozafarinia R, *et al*. The influence of laser treatment on hot corrosion behavior of plasma-sprayed nanostructured yttria stabilized zirconia thermal barrier coatings. *J Eur Ceram Soc* 2014, **34**: 2013–2021.
[23] Yi P, Mostaghimi J, Pershin L, *et al*. Effects of laser surface remelting on the molten salt corrosion resistance of yttria-stabilized zirconia coatings. *Ceram Int* 2018, **44**: 22645–22655.
[24] Soleimanipour Z, Baghshahi S, Shoja-Razavi R, *et al*. Hot corrosion behavior of Al_2O_3 laser clad plasma sprayed YSZ thermal barrier coatings. *Ceram Int* 2016, **42**: 17698–17705.
[25] Wang Y, Darut G, Luo XT, *et al*. Influence of preheating processes on the microstructure of laser glazed YSZ coatings. *Ceram Int* 2017, **43**: 4606–4611.
[26] Fan ZJ, Wang KD, Dong X, *et al*. The role of the surface morphology and segmented cracks on the damage forms of laser re-melted thermal barrier coatings in presence of a molten salt (Na_2SO_4+V_2O_5). *Corros Sci* 2017, **115**: 56–67.
[27] Yan Z, Guo L, Li ZH, *et al*. Effects of laser glazing on CMAS corrosion behavior of Y_2O_3 stabilized ZrO_2 thermal barrier coatings. *Corros Sci* 2019, **157**: 450–461.
[28] Guo L, Li MZ, Ye FX. Phase stability and thermal conductivity of RE_2O_3 (RE=La, Nd, Gd, Yb) and Yb_2O_3 co-doped Y_2O_3 stabilized ZrO_2 ceramics. *Ceram Int* 2016, **42**: 7360–7365.
[29] Zhang CL, Li MZ, Zhang YC, *et al*. Hot corrosion behavior of $(Gd_{0.9}Sc_{0.1})_2Zr_2O_7$ in V_2O_5 molten salt at 700–1000 °C. *Ceram Int* 2017, **43**: 9041–9046.
[30] Li MZ, Cheng YX, Guo L, *et al*. Preparation of nanostructured $Gd_2Zr_2O_7$–$LaPO_4$ thermal barrier coatings and their calcium-magnesium-alumina-silicate (CMAS) resistance. *J Eur Ceram Soc* 2017, **37**: 3425–3434.
[31] Wang JS, Sun JB, Zou BL, *et al*. Hot corrosion behaviour of nanostructured zirconia in molten $NaVO_3$ salt. *Ceram Int* 2017, **43**: 10415–10427.
[32] Loghman-Estarki MR, Nejati M, Edris H, *et al*. Evaluation of hot corrosion behavior of plasma sprayed scandia and yttria co-stabilized nanostructured thermal barrier coatings in the presence of molten sulfate and vanadate salt. *J Eur Ceram Soc* 2015, **35**: 693–702.
[33] Gok MG, Goller G. Microstructural evaluation of laser remelted gadolinium zirconate thermal barrier coatings. *Surf Coat Technol* 2015, **276**: 202–209.
[34] Ahmadi-Pidani R, Shoja-Razavi R, Mozafarinia R, *et al*. Laser surface modification of plasma sprayed CYSZ thermal barrier coatings. *Ceram Int* 2013, **39**: 2473–2480.
[35] Ahmadi-Pidani R, Shoja-Razavi R, Mozafarinia R, *et al*. Improving the hot corrosion resistance of plasma sprayed ceria–yttria stabilized zirconia thermal barrier coatings by laser surface treatment. *Mater Des* 2014, **57**: 336–341.
[36] Lima R, Kucuk A, Berndt C. Integrity of nanostructured partially stabilized zirconia after plasma spray processing. *Mat Sci Eng A* 2001, **313**: 75–82.
[37] Rahaman M, Gross J, Dutton R, *et al*. Phase stability, sintering, and thermal conductivity of plasma-sprayed ZrO_2–Gd_2O_3 compositions for potential thermal barrier coating applications. *Acta Mater* 2006, **54**: 1615–1621.
[38] Zhong XH, Wang YM, Xu ZH, *et al*. Hot-corrosion behaviors of overlay-clad yttria-stabilized zirconia coatings in contact with vanadate–sulfate salts. *J Eur Ceram Soc* 2010, **30**: 1401–1408.
[39] Guo L, Zhang CL, Li MZ, *et al*. Hot corrosion evaluation of Gd_2O_3–Yb_2O_3 co-doped Y_2O_3 stabilized ZrO_2 thermal barrier oxides exposed to Na_2SO_4+V_2O_5 molten salt. *Ceram Int* 2017, **43**: 2780–2785.